Exploring biogenic secondary organic aerosol using a PTRMS-CHARON in laboratory experiments: characterization and fingerprint analysis

Carolina Ramírez-Romero[1,2,a], Olatunde Murana[2], Hichem Bouzidi[2,b], Marina Jamar[2], Sébastien Dusanter[2], Alexandre Tomas[2], Ahmad Lahib[2,c],Layal Fayad[2,d], Véronique Riffault[2], Christopher Pöhlker[1], Stéphane Sauvage[2], and Joel F. de Brito[2]

[1]Multiphase Chemistry Department, Max Planck Institute for Chemistry, 55128 Mainz, Germany
[2]IMT Nord Europe, Institut Mines-Télécom, Université de Lille, Centre for Energy and Environment, 59000 Lille, France

[a] now at: Department of Chemistry, University of Toronto, Toronto, Canada
[b] now at: Université Paris Cité and Univ Paris Est Creteil, CNRS, LISA, F-75013 Paris, France
[c] now at: GRIMM Aerosol Technik, Ainring, Germany
[d] now at: Aix Marseille Univ, CNRS, LCE, 13331 Marseille, France

Correspondence to: Joel F. de Brito (joel.brito@imt-nord-europe.fr) and Carolina Ramírez-Romero (carolina.ramirezromero@utoronto.ca)

Abstract. Volatile Organic Compounds (VOC), particularly of biogenic origin emitted by vegetation and soils, play an important role in the global Organic Aerosol (OA) budget. The introduction of field-deployable Aerosol Mass Spectrometers in the early 2000s, combined with statistical analysis of their mass spectra, has significantly improved our understanding of the impact of secondary processes on fine-mode aerosol concentrations. While delivering innovative and significant insights, those analyses usually fail to explicitly identify precursors/mechanisms. In this context, this work focuses on laboratory-generated secondary OA (SOA) of biogenic VOC and its spectral analysis through a new generation of aerosol mass spectrometers, notably a Proton Transfer Reaction Mass Spectrometer coupled to a Chemical Analysis of AeRosol Online (PTRMS-CHARON) inlet. Aerosol particles were formed in the new DouAir atmospheric chamber via isoprene (ISOP) OH oxidation, monoterpene O_3 (limonene, MT), and sesquiterpene O_3 (β-caryophyllene, SQT) oxidation. ISOP experiments targeted "low-NO" environments, typically remote forested tropical areas, via epoxidiols formation (ISOP-IEPOX-SOA), or through an alternative branching favored in the absence of acidic seed particles (ISOP-non-IEPOX-SOA) and "high NO" environments, representative in urban and polluted regions (ISOP-NO-SOA). Experiments showed that those five SOA formation pathways (ISOP-IEPOX-SOA, ISOP-non-IEPOX-SOA, ISOP-NO-SOA, and the ozonolysis reactions of MT and SQT) exhibited distinguishable spectra, with identifiable tracer ions, such as *m/z* 119.07 ($C_5H_{10}O_3$), *m/z* 137.081 ($C_5H_{12}O_4$) for ISOP-IEPOX-SOA, $C_5H_{10}O_4$ (*m/z* 135.070), $C_5H_{10}O_6$ (*m/z* 167.055) for ISOP-non-IEPOX-SOA, and *m/z* 85.028 ($C_4H_4O_2$) for NO-SOA pathways, as well as molecules with C_7-C_{10} and C_7-C_{15} structures, including characterisitic fragments, identified during MT and SQT oxidation experiments, respectively. Notably, *m/z* 83.049 (C_5H_6O) was detected in both low-NO isoprene pathways, suggesting a broader diagnostic role. These laboratory findings depict promising results for ambient near-real-time biogenic SOA source apportionment, notably in forested and/or urbanized areas.

1. Introduction

Globally, organic aerosol (OA) particles account for an average of ~50 % of the submicron particulate matter (PM_1), however, with values ranging from 10 to 90 %, depending on the nature of the site (forested, urbanized, etc.) and atmospheric conditions (de Gouw and Jimenez, 2009; Tsimpidi et al., 2025). PM largely affects radiative forcing, climate, air quality, and public health, and has therefore been the subject of intense research (Hallquist et al., 2009; Shrivastava et al., 2017; Nault et al., 2021; Pye et al., 2021). While primary sources contribute to this burden, a dominant fraction originates from the atmospheric oxidation of volatile organic compounds (VOC), with biogenic VOC (BVOC) being widely accepted as the most significant precursors globally (Yáñez-Serrano et al., 2020; Dada et al., 2023). The chemical complexity of biogenic secondary organic aerosol (BSOA) formation is high. Terpenoids such as monoterpenes and sesquiterpenes are key precursors in boreal environments due to their rapid reactivity (Hakola et al., 2012; Zhou et al., 2017; Roldin et al., 2019). Conversely, in tropical regions like the Amazon, isoprene dominates emissions, where its oxidation pathways, varying drastically between low-NO and high-NO conditions, dictate the resulting aerosol composition (Martin et al., 2010; Leppla et al., 2025). Unraveling these distinct chemical pathways requires precise identification of the oxidation products, which serve as unique tracers for source apportionment.

Mass spectrometric techniques such as Aerosol Mass Spectrometers (AMS) have been extensively used in the scientific community to understand OA loadings and dynamics (Hu et al., 2015; Kristensen et al., 2017). However, the high fragmentation associated with electron impact ionization hinders molecular characterization and reduces the source/process identification capabilities. In recent years, new soft ionization techniques have been implemented in mass spectrometry techniques to reduce fragmentation, allowing the identification of low-volatility compounds at the molecular level, such as chemical ionization mass spectrometry (CI-MS) (Lopez-Hilfiker et al., 2014; Eichler et al., 2015). Molecular ionization is achieved by the transfer of an electron/proton/adduct of various reagent ions (e.g., Br^-, H_3O^+, NH_4^+, I^-, Huang et al., 2021). CI-MS equipped with a H_3O^+ source (Proton-Transfer-Reaction Mass Spectrometry, PTR-MS) has been the main tool for fast and precise quantification of small organic gaseous compounds for several decades (de Gouw and Warneke, 2007). More recently, the system has been coupled with thermo-desorption (TD) aerosol inlets, termed CHemical Analysis of aeRosol ONline (CHARON-PTRMS, Eichler et al., 2015).

However, the application of CHARON to date has left specific gaps regarding BSOA. Previous field deployments have successfully quantified bulk OA or identified specific tracers in urban and biomass burning plumes (Müller et al., 2017; Piel et al., 2019; Song et al., 2024). Similarly, laboratory applications have largely focused on anthropogenic precursors like toluene (Lannuque et al., 2023) or vehicle emissions (Kostenidou et al., 2024). While isolated studies have touched upon biogenic precursors (Gkatzelis et al., 2018a, b), a comprehensive spectral library covering the major isoprene and terpene oxidation pathways is lacking.

To address this gap, we characterized the formation of SOA from the most relevant biogenic precursors in the new Teflon DouAir atmospheric chamber. We systematically investigated five distinct SOA formation pathways, namely monoterpene (limonene) and sesquiterpene (β-caryophyllene) ozonolysis, the isoprene-OH oxidation via the HO_2 route, favoring or suppressing the epoxidiol route (IEPOX-SOA and non-IEPOX-SOA) under low-NO conditions, and the isoprene-NO oxidation promoting the isoprene-NO-SOA in high polluted environments.

2. Materials and methods

2.1. DouAir Atmospheric Simulation Chamber

The experiments were conducted in the new 9 m^3 mobile DouAir Teflon chamber (Fig. 1), housed at IMT Nord Europe, Douai, France. The chamber, made of fluorinated ethylene propylene (FEP) Teflon, allows the study of multiple atmospheric processes, including OH reactivity, peroxy radical chemistry, and aerosol formation, both in laboratory settings and field deployments. DouAir can be operated under dark conditions or irradiated either via natural solar light or artificial UV lamps, allowing the simulation of a wide range of atmospheric conditions. The chamber is equipped with 48 UVA actinic lamps (365 nm, 40 W, 1.2 m in length), with 24 lamps mounted on each side. The photolysis frequency for NO_2, $J(NO_2)$, was determined by actinometry and measured to be 1.42 × 10^{-3} s^{-1}.

Its injection line can be heated up to 100 °C to optimize the introduction of compounds with a wide range of volatilities. The mixing time of gases is less than 4 minutes in the chamber (Supplementary Information, SI). A zero-air generator (AZ purifier 2020, Claind) coupled to a humidification system provides continuously zero air to compensate for the sampling flow rate of the analytical instruments as well as to control the relative humidity (RH), typically ranging from 8 L min^{-1} up to 40 L min^{-1}. The chamber is equipped with a large array of analytical instruments focusing on VOC, aerosol particles, and atmospheric radicals, sampling from the opposite side of the injection ports. The supplementary material presents the DouAir chamber characteristics, including mixing time and wall loss correction factors for various species.

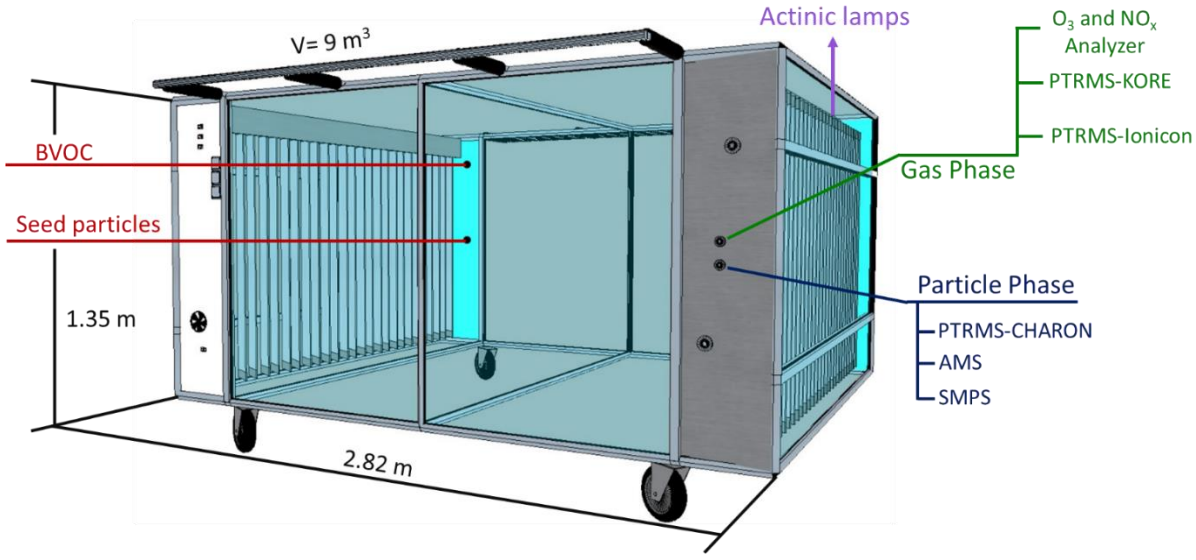

Figure 1: Schematics of the DouAir chamber depicting instrument layouts, ports, and injection points.

2.2. Instruments

The CHARON system (Ionicon Analytik Inc, Innsbruck., Austria) is an aerosol inlet for the chemical characterization of sub-micrometer particles larger than ~125 nm. The system consists of a gas-phase denuder, a critical orifice, and an aerodynamic lens (enrichment factor, EF ~21) focusing particles into a thermo-desorption unit (TDU) at 140 °C at a pressure of typically 8 mbar (Müller et al., 2014). Determination of the instrumental background is done automatically by switching the sampled air flow through a HEPA filter.

The CHARON inlet is coupled here to a quadrupole interface PTRMS (PTR-QiTOF-MS; Ionicon Analytik Inc, Innsbruck, Austria; Müller et al., 2014). The pressure and temperature in the drift tube were 2.6 mbar and 80 °C, respectively. Voltages in the drift tube were set to achieve 80 Td and 100 Td for the particle and gas phase measurements, respectively. These electric fields (1Td = 10^{-17} V cm^2) determine the kinetic energy of the ions within the drift region, largely preventing the formation of water clusters but potentially leading to the fragmentation of target molecules. Lower E/N values for the particle phase were possible due to water removal by the CHARON denuder. To ensure high mass accuracy and confidence in molecular formula identification, mass calibration was performed internally using four ubiquitous peaks spanning the measured mass range. These included the hydronium water isotope (H_3O^+ at *m/z* 21.022), the second water cluster (at *m/z* 55.039), and the diiodobenzene peaks ($C_6H_5IH^+$ at *m/z* 203.943 and $C_6H_4I_2H^+$ at *m/z* 330.848). This continuous internal calibration resulted in a mass accuracy of better than 5 ppm across the detection range.

The gas phase calibration of the PTRMS ion transmission curve was performed using a Gas Calibration Unit (Ionicon Analytik Inc., Innsbruck, Austria) coupled to a certified gas cylinder (National Physical Laboratory; Worton et al., 2023) with RH levels comparable to the chamber experiments (15-50%). The gas cylinder contained compounds ranging up to 370 amu, including hydrocarbons (e.g., benzene, toluene, *m*-xylene) and oxygenated molecules (e.g., acetaldehyde, methyl ethyl ketone (MEK), and octamethylcyclotetrasiloxane). The quantification of particle-phase concentration requires, in addition to accurate gaseous calibration, the determination of the EF (i.e., the efficiency of particle enrichment before evaporation in the TDU and introduction into the drift tube) described in Eichler et al. (2015). The theoretical EF is defined as the ratio of the volumetric sampling flow rate entering the Aerosol Dynamic Lens (ADL) to the volumetric flow rate entering the drift tube. However, to account for transmission efficiency and wall losses, the experimental size-dependent EF was determined by introducing a known number concentration of monodispersed particles, as described in Eichler et al. (2015) and Peng et al. (2023). In this study, ammonium nitrate (NH_4NO_3) and levoglucosan ($C_6H_{10}O_5$) particles were used for calibration with solutions at concentrations of 0.005 M and 0.01 M, respectively. The solutions were nebulized using an atomizer (TSI 3080), and the resulting polydisperse particles were size-selected (100 nm - 400 nm) using a differential mobility analyzer (DMA; TSI 3082). The monodisperse particles were sampled by a condensation particle counter (CPC; TSI 3750) and the PTRMS-CHARON. The mass concentration of size-selected particles measured by the CPC was determined assuming a shape factor of 0.8 and 1 for ammonium nitrate and levoglucosan, respectively. This mass concentration was subsequently converted into a Volume Mixing Ratio (VMR, in ppbv). Finally, the size-dependent EF was calculated as the ratio between the VMR measured by the PTRMS-CHARON and the equivalent VMR derived from the CPC data. The EF using levoglucosan (a non-volatile marker) yielded an EF of 24.1 ± 0.5, demonstrating efficient particle enrichment. In contrast, semi-volatile ammonium nitrate yielded a significantly lower EF (~6.5 ± 1.2), likely due to particle evaporation within the sub-atmospheric pressure region of the CHARON inlet. Given that the measured EF for stable particles (24.1) was in reasonable agreement with the theoretical EF, as well as the manufacturer's certified documentation (21), the latter was applied to all datasets.

Depending on the experimental protocol, the instrument was either operated in particle-phase sampling mode exclusively or in alternating 40 minutes particle-phase and 20 minutes gas-phase cycles. PTRMS-CHARON data was processed using the Viewer software (Version 3.4.4, IONICON). This software was used to perform the calculation of transmission curves, and the peaks deconvolution and mass calibration on the spectrum. The

molecular composition was determined based on accurate mass-to-charge ratios (m/z) for the ions detected. Primary ion information, and other operational parameters such as drift tube pressure, and voltages, were considered for the calculation of mixing ratios in ppbv. Further data analysis, including the conversion to mass concentrations (ng m^{-3}), was carried out using custom MATLAB scripts (The MathWorks Inc., Natick, MA, USA), as described in the SI.

Other mass spectrometers were used to complement PTRMS-CHARON observations, such as a second PTRMS (second generation, Kore Technology Inc.; Michoud et al., 2017) for VOC measurements during ISOP-SOA and MT-SOA experiments. This PTRMS was operated with an E/N = 130 Td, maintaining pressures of 2.2 mbar and 1.4 mbar in the glow discharge and reactor, respectively. A VOC calibration procedure similar to PTRMS-CHARON was performed, and, for some of the experiments, a High-Resolution Aerosol Mass Spectrometer (HR-AMS, Aerodyne Research Inc.; DeCarlo et al., 2006) operated in V-mode at 30 s time resolution was coupled to the chamber. Data has been treated with the Peak Integration by Key Analysis (PIKA) module, and frequent blanks during the experiments were used to correct for fluctuations in the CO_2^+ signal at m/z 44. The HR-AMS has been calibrated using monodispersed ammonium nitrate and ammonium sulfate particles from the corresponding solutions at 0.005 M. HR-AMS data were corrected using the parametrization of Middlebrook et al. (2012). A collection efficiency (CE) of 1.0 was used for the ISOP-IEPOX-SOA experiment, due to the presence of acidic seed particles, while a CE of 0.5 was applied to the ISOP-non-IEPOX-SOA and ISOP-NO-SOA experiments with neutral seed aerosol. Ancillary instrumentation consisted of a scanning mobility particle sizer (SMPS, model 3082 coupled to a butanol CPC 3750 at a range of 7 - 283 nm, TSI), an ozone monitor (POM model 202, 2B technologies), a NO_x analyzer (T200UP, Teledyne), and a RH monitor (LI-840A, Li-COR).

2.3 Experimental protocol

Three different terpenoids were used as precursors for SOA production: isoprene (ISOP, Sigma-Aldrich, 99%), limonene (MT, Sigma-Aldrich, 97%), and β-caryophyllene (SQT, Sigma-Aldrich, > 80%). All experiments were conducted at 15–50% RH and roughly 20 °C. Following each experiment, the DouAir chamber was flushed with purified air (40 L min^{-1}) for at least 24 hours. Table 1 summarizes the specific conditions for each experiment.

Isoprene experiments

ISOP-SOA formation was investigated under three configurations: ISOP-IEPOX, ISOP-non-IEPOX, and ISOP-NO-SOA:

- Low-NO Conditions (IEPOX/non-IEPOX): Hydroxyl radicals (OH) were generated via tetramethylethylene (TME, C_6H_{12}) ozonolysis, as described in Berndt et al. (2019). The OH concentration was calculated based on the decay of the dilution-corrected isoprene signal, following the approach described by Barmet et al. (2012) and detailed in the SI. Seed particles and the initial ozone injection were introduced prior to isoprene addition. To maintain ozone concentrations between 100–110 ppbv, additional ozone was injected as needed, and TME was injected every 5 minutes for approximately 4 hours. The ISOP-IEPOX-SOA experiments utilized acidic seed particles (0.005 M ammonium sulfate + 0.1 M sulfuric acid) at 50% RH, with continuous seed injection to maintain acidity. The ISOP-non-IEPOX-SOA experiments used neutral seed particles (0.005 M ammonium sulfate) at 15–30% RH.

- High-NO Conditions (ISOP-NO-SOA): OH was generated via HONO photolysis. These experiments employed neutral seed particles (0.005 M ammonium sulfate) and initial mixing ratios of NO (~8 ppbv) and NO_2 (~5 ppbv).

Monoterpene and sesquiterpene experiments

MT-SOA and SQT-SOA were generated via the ozonolysis of limonene and β-caryophyllene, respectively, without seed particles. For all experiments, chamber humidification was the initial step, followed by background measurements. Ozone was injected prior to the precursor.

- Limonene (MT): Three injections were performed at 20-minute intervals.
- β-caryophyllene (SQT): Seven injections were performed at intervals between 20 and 45 minutes.

Table 1. Summary of experimental conditions during the chamber experiments. Maximum SOA mass concentrations were determined using AMS for the ISOP-SOA experiments and SMPS for the MT- and SQT-SOA experiments.

Experiment (# of repetitions)	Seed particles	Injection of biogenic precursor in ppbv (# of injections)	Ozone (ppbv)	Injection of TME in ppbv (# of injections)	OH (molecules cm^{-3})	RH (%)	NO and NO_2 (ppbv)	Maximun SOA formed (μgm^{-3})	SOA formation conditions
ISOP-IEPOX-SOA (3)	$(NH_4)_2SO_4$+H_2SO_4	200 (1)	80-100	10 (27)	~4 x 10^5	50	< 1	~5	Reaction with OH
ISOP-non-IEPOX- SOA (2)	$(NH_4)_2SO_4$	100 (2)	80-100	10 (19)	~4 x 10^5	15-30	< 1	~4	Reaction with OH
ISOP-NO-SOA (1)	$(NH_4)_2SO_4$	90 (1)	~100	----	~4 x 10^6	30	7.5 and 5.3	~3	Reaction with OH
MT-SOA (5)	----	18 (3)	80 initial	----	----	30	----	~120	Ozonolysis
SQT-SOA (3)	----	10 (7)	100 initial	----	----	30	----	~83	Ozonolysis

3. Results and discussion

The concentration of gas and particulate species during the BSOA formation experiments are shown in Figure 2. For the ISOP-SOA experiments, the time t = 0 refers to the first injection of the seed particles, while for MT and SQT, it refers to the first injection of the biogenic precursor. Fig. 2 shows the concentration of VOC precursors, namely isoprene (*m/z* 69.07), limonene (*m/z* 81.07 and *m/z* 137.131), and β-caryophyllene (*m/z* 81.070, 95.086, 109.101, 123.117, 135.117, 137.131, 149.132, and 205.195; Kim et al., 2009). The precursor gas concentration peaked at ~190 ppbv, ~220 ppbv, ~90 ppbv for ISOP-IEPOX-, ISOP-non-IEPOX-, and ISOP-NO-SOA experiments, respectively, ~40 ppbv for MT (injections totaling 72 ppbv), whereas the maximum SQT concentration has been roughly 5 ppbv for a total injected of 70 ppbv, due to its high reactivity. To minimize the formation of new particles (nucleation events), sequential injections of MT and SQT were employed. This approach promoted the condensation and reactive uptake of semi-volatile compounds onto the pre-existing seed particles formed during the initial injection. Consequently, the large difference between the total MT and SQT injected levels and those observed in the chamber is associated with the high reactivity of MT and SQT with O_3, leading to fast consumption once injected in the chamber. Additional factors that may contribute to these differences include losses on the chamber walls and inside the PTRMS inlet. In the ISOP-NO-SOA experiment, a peak of ~300 ppbv isoprene was observed at first detection, stabilizing to 90 ppbv for 2 min, ensuring proper mixing in the chamber.

The first-oxidation products of the biogenic precursors are also shown in Fig. 2. For ISOP, the depicted compounds are methyl-vinyl ketone (MVK, C_4H_6O), methacrolein (MACR, C_4H_6O), and ISOPOOH ($C_5H_{10}O_3$), their sum being detected at *m/z* 71.049 (Liu et al., 2013; Bernhammer et al., 2017). The oxidation products of MT shown here are levulinic acid ($C_5H_8O_3$, *m/z* 117.055 + *m/z* 99.044), limonalic acid, norlimononic acid, and ketolimononaldehyde ($C_9H_{14}O_3$, *m/z* 171.102 + *m/z* 153.091) (Gkatzelis et al., 2018a, b). The selected SQT oxidation products were β-caryophyllinic acid ($C_{14}H_{22}O_4$, *m/z* 255.159 + *m/z* 237.149), β-caryophyllon aldehyde ($C_{15}H_{24}O_2$, *m/z* 237.185 + *m/z* 219.174) and β-caryophyllonic acid ($C_{15}H_{24}O_3$, *m/z* 253.180 + *m/z* 235.169) (Li et al., 2011; Chan et al., 2011; Gao et al., 2022). It is important to mention the stepwise increases ("modes") in OA concentration during ISOP-IEPOX-SOA and ISOP-non-IEPOX-SOA reflect bursts of SOA formation driven by oxidant availability rather than the number of isoprene injections. Because OH radicals were generated through discrete O_3 injections for TME ozonolysis, each addition of O_3 triggered a new period of rapid SOA formation, producing the observed modes in the OA time series.

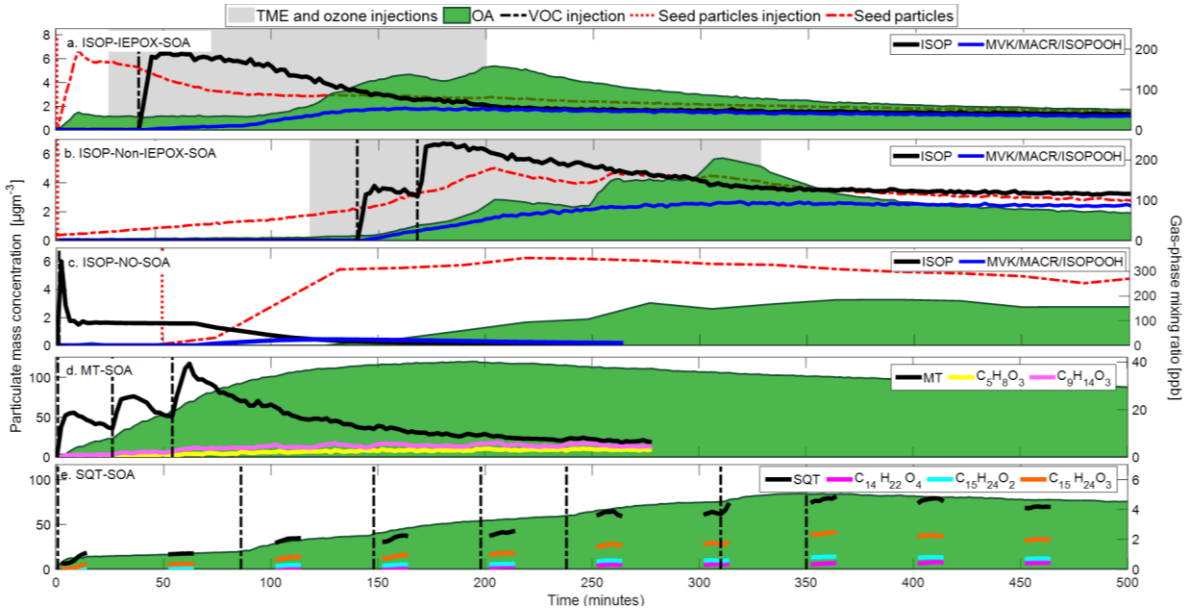

Figure 2: Concentration of particulate and gaseous species during the following experiments: (a) ISOP-IEPOX-SOA, (b) ISOP-non-IEPOX-SOA, (c) ISOP-NO-SOA, (d) MT-SOA, and (e) SQT-SOA. Seed particles are shown in red, SOA in green, and the gaseous precursors in black, while gas-phase oxidation products are color-coded by experiment. The vertical red and black dashed lines represent the injection of seed particles and VOC precursors, respectively, and the grey areas correspond to OH production via O_3 + TME injections. The seed particle signal was divided by 4 and 2 for ISOP-IEPOX and ISOP-non-IEPOX-SOA experiments, respectively, for better visualization. The SQT mixing ratios in panel d have been calculated as the sum of signals at *m/z* 81.070, 95.086, 109.101, 123.117, 135.117, 137.131, 149.132, and 205.195. Measurements of gas precursors in the SQT experiments are discontinuous due to the switching between gas and particle phase measurements in the PTRMS-CHARON.

To characterize the contribution of IEPOX-SOA and to distinguish it from the ISOP-non-IEPOX-SOA pathway, we used the established AMS marker $f_{C_5H_6O}$, defined as the ratio of C_5H_6O (m/z 82 at unit mass

resolution) to total OA (Hu et al., 2015). This ion corresponds to methyl furan, a thermal decomposition product of 3-MeTHF-3,4-diols formed via IEPOX reactive uptake (Robinson et al., 2011; Lin et al., 2012; Hu et al., 2015). Additionally, f_{CO_2} (or f_{44} at unit mass resolution) was used to evaluate the OA oxidation state and degree of aging (Cubison et al., 2011; Milic et al., 2017; Morgan et al., 2020). As shown in Fig. 3, $f_{C_5H_6O}$ increased substantially under IEPOX-reactive uptake conditions compared to the ISOP-non-IEPOX-SOA pathway, confirming the formation of IEPOX-derived aerosol. This enhancement is driven by the acidity of the seed particles, which catalyzes the ring-opening of the epoxide functional group, accompanied by the addition of particle-phase nucleophiles such as sulfate and water (Liu et al., 2015; Wong et al., 2015). The RH also played an important role in the reactive uptake of IEPOX. Wong et al. (2015) demonstrated that under high-RH conditions, particle-phase water strongly enhances SOA formation. These conditions promote the dissolution of soluble species, facilitating aqueous-phase oxidation and leading to the formation of low-volatility products such as C_5-alkene triols (e.g., 2-methyltetrols and $C_5H_{10}O_3$ compounds; Frauenheim et al., 2022), 1,4-diols, 1,3-diols, 3-methyltetrahydrofuran-3-ol, oligomers, and organosulfates (Kuwata et al., 2015; Liu et al., 2015; D'Ambro et al., 2019). In the case of the non-IEPOX-SOA pathway, highly oxidized compounds are formed even in the absence of reactive aqueous seed particles, enhancing the formation of molecules such as $C_5H_{10}O_5$, $C_5H_{12}O_5$, and $C_5H_{10}O_6$ (Liu et al., 2016). In Figure 3, laboratory experiment results from previous studies related to ISOP-IEPOX-SOA are also included for comparison (Lin et al., 2012; Budisulistiorini et al., 2013; Canagaratna et al., 2015; Kuwata et al., 2015; Liu et al., 2015). The results indicate that the protocol applied here, mainly associated with seed particle acidity and RH, successfully isolated the IEPOX-SOA regime from the standard low-NO oxidation pathway.

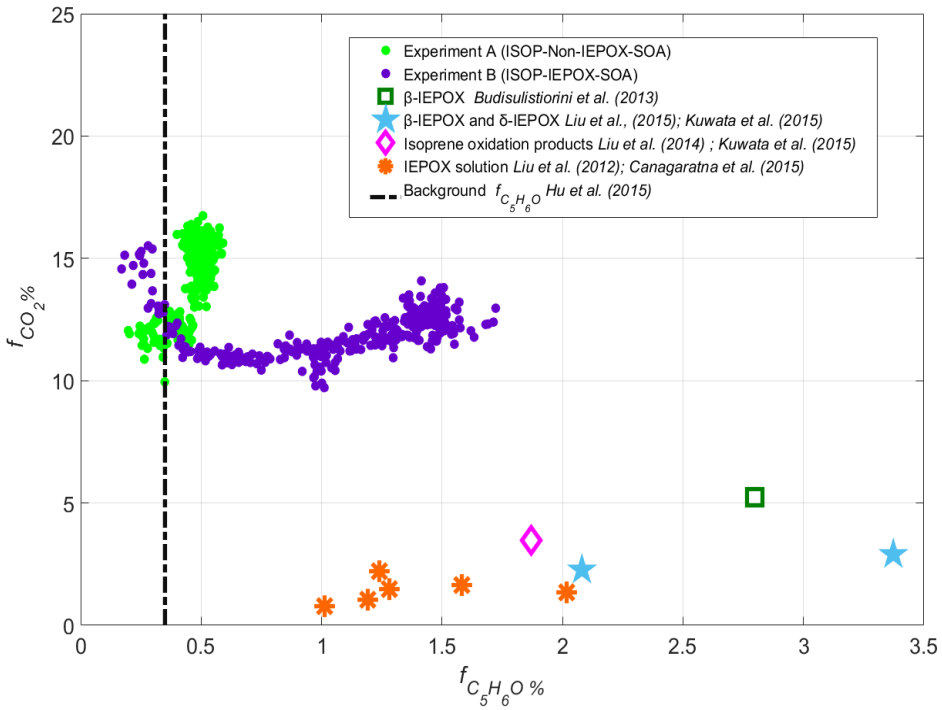

Figure 3: AMS scatter plot of f_{CO_2} vs. $f_{C_5H_6O}$ (expressed in percentage, %) for ISOP-SOA experiments conducted in the DouAir atmospheric chamber. The successful production of IEPOX-SOA was achieved by increasing relative humidity (from 20% to 50%) and using acidic seed particles. For comparison, data

from literature laboratory experiments characterizing IEPOX uptake and isoprene oxidation pathways are also included.

Figure 4 shows the time series of the aerosol concentration on the ISOP-IEPOX-SOA experiment, as well as CHARON observations of *m/z* 119.07 ($C_5H_{10}O_3$) and *m/z* 137.081 ($C_5H_{12}O_4$), referred to as "C_5-alkene triols", previously reported in the literature as tracers of IEPOX-SOA (Frauenheim et al., 2022; Lopez-Hilfiker et al., 2016; D'Ambro et al., 2019). The initial offset between the AMS and CHARON signals is attributed to a residual organic background on the seed particles, which is detected immediately by the AMS as bulk mass, whereas the CHARON tracers track the kinetic induction of fresh oxidation products. In addition, it is interesting to note the *m/z* 83.049 (C_5H_6O) detected in PTRMS-CHARON also has a high signal, especially during the second injection of acid particles, when mass concentrations increased, suggesting a similar process of IEPOX-SOA identification as through AMS (Hu et al., 2015).

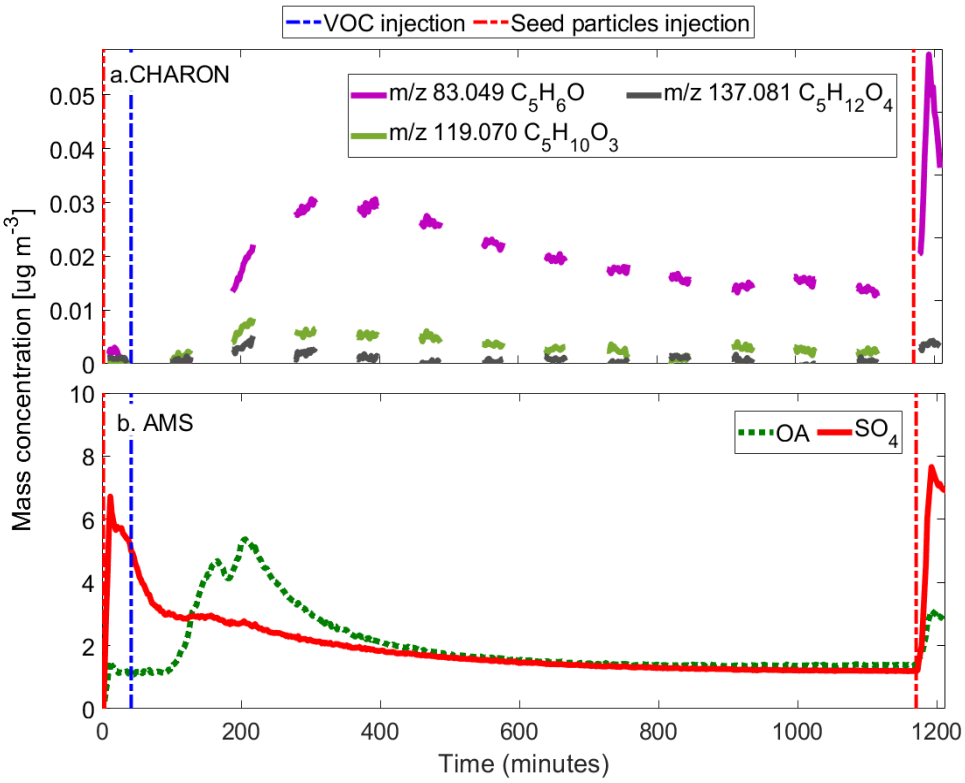

Figure 4: Time series of (a) selected ions detected by PTRMS-CHARON during the ISOP-IEPOX-SOA experiment and (b) aerosol mass concentrations measured by AMS. The measurements in panel (a) are discontinuous due to the switching between gas and particle phases in the PTRMS-CHARON.

Figure 5 depicts the signature spectrum for the experiments studied here. For ISOP-non-IEPOX-, MT-, and SQT-SOA, the signature spectra were extracted from the period corresponding to the maximum OA concentration (corrected for wall losses and dilution). This period was identified as a period of chemical stability, representing the mature SOA composition. For ISOP-IEPOX-SOA, the signature spectrum was selected during the second injection of acidic seed particles, after the onset of gas-phase oxidation, when the C_5H_6O signal measured by CHARON reached the highest concentration.

Panel (a) shows the fingerprint for ISOP-IEPOX-SOA, notably dominated by C_5H_6O, $C_2H_4O_3$ (m/z 77.023), $C_5H_8O_4$ (m/z 133.05), and $C_9H_{12}O_3$ (m/z 169.086). Mettke et al. (2023) showed that $C_5H_8O_4$ is a product of the uptake of hydroxy hydroperoxide (ISOPOOH), formed via OH oxidation of ISOP, generating isoprene-hydroxy-peroxy radicals (ISOPOO), which subsequently react bimolecularly with HO_2 to form ISOPOOH. The $C_5H_8O_4$ compound was also found in the formation of SOA from standardized isomers of ISOPOOH and from isoprene oxidation (Krechmer et al., 2015; D'Ambro et al., 2017). The ion $C_5H_8O_2$ (m/z 101.060) was also observed here and can be associated with the fragmentation of $C_5H_{10}O_3$ (shown in Fig. 4) through a dehydration process.

Generally, the average spectrum of ISOP-non-IEPOX-SOA (Fig. 5b) also depicts major contributions from C_5 compounds, with some overlapping ions such as $C_5H_8O_2$, $C_5H_8O_4$, $C_5H_6O_2$ (*m/z* 99.044), and $C_5H_8O_3$ (*m/z* 117.055), but differing relative contributions. The latter, more strongly identified in the ISOP-non-IEPOX-SOA pathway, might be a fragment of $C_5H_{10}O_4$ (*m/z* 135.070), identified in the literature as a marker of ISOP-non-IEPOX-SOA (Mettke et al., 2023). Similarly, $C_5H_8O_2$ may be enhanced via fragmentation of $C_5H_{10}O_3$ (*m/z* 119.07), although the latter was not observed here. $C_5H_{10}O_6$ (*m/z* 167.055), a known product of the reactive uptake of ISOPOOH in the ISOP-non-IEPOX-SOA pathway, was identified here (Liu et al., 2016; Mettke et al., 2023). $C_5H_{10}O_5$, $C_5H_{12}O_5$, and $C_5H_{12}O_6$, also cited in the literature, however, were not observed during those experiments. It is important to note that CHARON also detects C_5H_6O at the ISOP-non-IEPOX-SOA route, contrary to HR-AMS. Our results suggest that the C_5H_6O ion measured with the CHARON inlet acts as a broader tracer for low-NO isoprene SOA, rather than being specific to the IEPOX pathway. Therefore, caution is warranted when using this ion as a tracer for ISOP-derived SOA in PTRMS-CHARON measurements, and a more comprehensive evaluation combining chamber and field studies is needed to confirm the robustness of this tracer.

Figure 5c shows that the spectrum of ISOP-NO-SOA is predominantly characterized by C_4 compounds, including $C_4H_4O_{2,3}$ (*m/z* 85.028; *m/z* 101.023), $C_4H_6O_{1,2}$ (*m/z* 71.049; *m/z* 87.044), and $C_4H_8O_{1,2}$ (*m/z* 73.065; *m/z* 89.060). The compound $C_4H_4O_2$, a fragment of $C_4H_6O_3$, has been previously reported in studies of ISOP-NO_x irradiation (Jia and Xu, 2018) and methacrolein (MACR)-NO_x irradiation (Lin et al., 2013). The mass ion $C_4H_6O_3$ has been identified as a fundamental unit in the oligomerization of 2-methylglyceric acid (2-MGA) in SOA formation, where it serves as a molecular tracer for ISOP-SOA (Kleindienst et al., 2007; Nguyen et al., 2011; Zhang et al., 2011). Among the C_5 compounds, $C_5H_6O_{1\text{-}2}$ (*m/z* 83.049; *m/z* 99.044), C_5H_8O (*m/z* 85.065) was detected, whereas C_5H_6O and C_5H_8O are typically dominant in low-NO ISOP-SOA. Their presence may be linked to the lower SOA yields associated with isoprene hydroxy nitrate formation (Jacobs et al., 2014). The mass ion $C_6H_8O_4$ (*m/z* 145.050) has similarly been identified by Schwantes et al. (2019), which was shown to result from the esterification of 2-MGA with acids in the particle phase (Chan et al., 2010). Mass ions $C_3H_4O_2$ (*m/z* 73.028) and $C_3H_6O_2$ (*m/z* 75.044) were detected at high intensities, with the latter previously identified as hydroxyacetone (Jia and Xu, 2018).

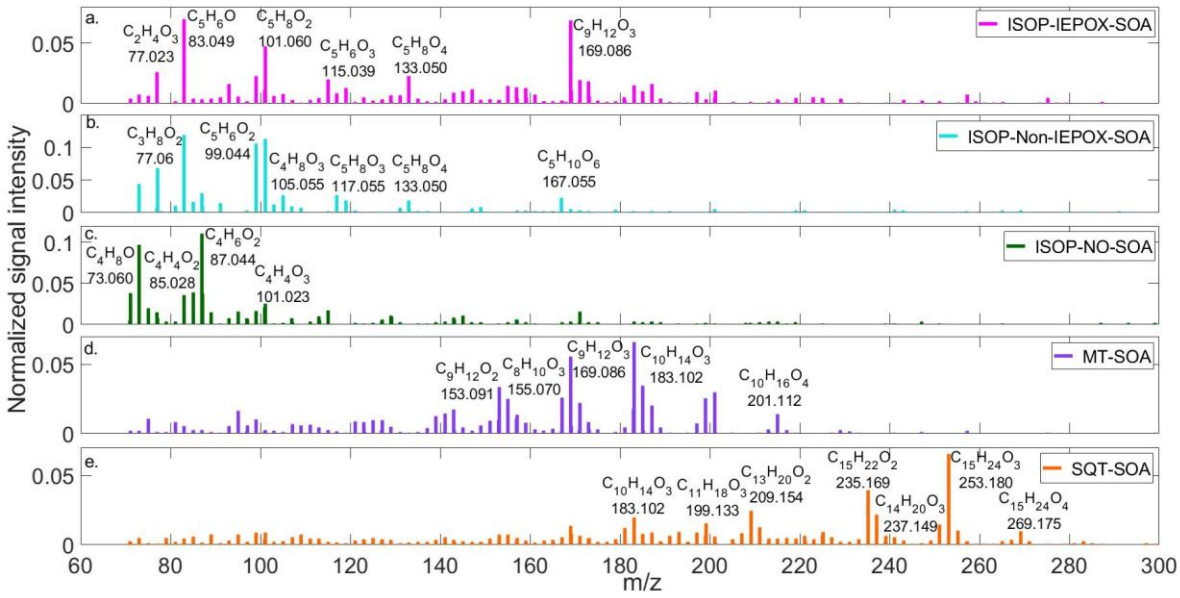

Figure 5: Signature spectra of (a) ISOP-IEPOX-SOA, (b) ISOP-non-IEPOX-SOA, (c) MT-SOA, (d) SQT-SOA as detected by PTRMS-CHARON.

Similar to the ISOP-SOA experiments, the contribution of compounds to MT- and SQT-SOA is distributed between main ions and likely fragments, several of which have been previously reported in the literature. Using PTRMS–CHARON, Gkatzelis et al. (2018a) observed highly oxidized semi-volatile compounds during limonene ozonolysis, including $C_8H_{12}O_{4,5}$, $C_9H_{14}O_{3,4}$, and $C_{10}H_{16}O_{3,4}$. These species were also detected in our MT-SOA experiments in the DouAir chamber, as well as their potential fragments (detailed in Table S2). The $C_9H_{14}O_{3,4}$ ions are attributed to multifunctional oxygenated C_9 products, dominated by carboxylic acids and aldehydes formed during limonene ozonolysis (Gkatzelis et al., 2018a; Jacob et al., 2023). These compounds are produced via alkoxy-radical (e.g., $C_9H_{13}O_3$) and RO_2 chemistry followed by intramolecular isomerization, as described by Kundu et al. (2012). The $C_9H_{12}O_4$ ion may also represent a fragmentation product of $C_9H_{14}O_5$ (m/z 203.091), a compound previously identified by Jacob et al. (2023) using liquid chromatography–mass spectrometry (LC-MS). The $C_{10}H_{16}O_{3,4}$ ions are attributed to larger multifunctional carboxylic acids and aldehydes (Gkatzelis et al., 2018a; Wong et al., 2021), while lower-carbon-number oxidation products (e.g., $C_8H_{12}O_{4,5}$) correspond to highly oxygenated C_8 carboxylic acids (Hammes et al., 2019; Jacob et al., 2023). During the SQT-SOA experiments, the composition was dominated by multifunctional oxygenated sesquiterpene products, consistent with previous PTRMS–CHARON observations of β-caryophyllene ozonolysis (Gao et al., 2022). The most abundant signals corresponded to $C_{15}H_{24}O_{2,3}$ and $C_{14}H_{22}O_{2,3}$ ions, typically associated with first-generation ozonolysis products such as aldehydes and carboxylic acids (Li et al., 2011). In addition, more highly oxygenated species, including $C_{15}H_{24}O_4$ and $C_{15}H_{26}O_4$, were detected and are consistent with hydroxy- and hydrated carboxylic acids formed (Chan et al., 2011; Li et al., 2011; Jaoui et al., 2013; Gao et al., 2022). Lower-carbon-number oxidation products (e.g., C_{11} compounds) were also observed, consistent with second-generation oxidation products formed during β-caryophyllene ozonolysis (Li et al., 2011; Jaoui et al., 2013). A comprehensive list of the detected main ions, their likely fragments, and corresponding compound assignments is provided in Table S3.

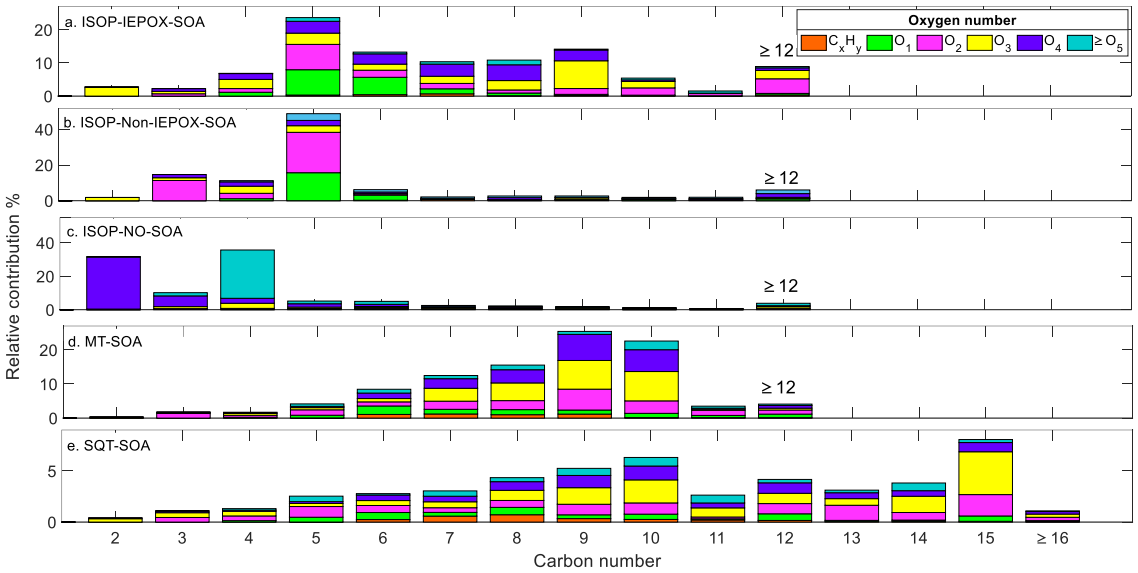

Figure 6: Relative contributions of the total OA fraction for (a) ISOP-IEPOX-SOA, (b) ISOP-non-IEPOX-SOA, (c) MT-SOA, and (d) SQT-SOA. The SOA fraction distribution is based on the number of carbons and oxygens in the detected ions.

The different SOA spectra obtained with PTRMS-CHARON have been studied according to their number of carbons and oxygens, as shown in Fig. 6. Following the results presented previously, ions associated with C_5 molecules/fragments dominated both ISOP-SOA pathways under low-NO conditions, being responsible for roughly ~50% and ~25% contribution in ISOP-non-IEPOX- and ISOP-IEPOX-SOA, respectively. The contribution of C_5 compounds in the non-IEPOX-SOA route is comparable to that reported by Liu et al. (2016a) using a FIGAERO HF-ToF-CIMS (52 %). D'Ambro et al. (2017) also observed the same behavior, attributing ~64% of the OA to C_5 compounds during the first hours of isoprene oxidation. On the other hand, C_4 molecules dominated the ISOP-NO-SOA experiment with ~35% of the total OA mass, followed by ~31% of C_2 molecules. The prominent C_2-C_4 molecules identified in this experiment share the same molecular skeletons as species reported in similar studies by Jia and Xu (2018).

The ISOP-IEPOX-SOA mass spectrum (Figure 6) exhibits a notably broader and more diverse molecular distribution compared to the non-IEPOX pathway. This complexity is likely driven by the formation and subsequent processing of low-volatility oligomers. Previous studies have established that acidic conditions promote the formation of non-sulfated dimers, such as $C_{10}H_{22}O_7$ and $C_{10}H_{20}O_6$ (Surratt et al., 2006; Lin et al., 2014). Furthermore, Armstrong et al. (2022) suggested that these oligomers can decompose via OH oxidation into lower molecular weight compounds. Although the PTR-MS/CHARON cannot directly resolve these high-mass oligomers, their decomposition, combined with ionic fragmentation within the drift tube, provides a plausible mechanism for the dense array of ions observed in the IEPOX-SOA spectrum.

The varied distribution of molecules in the mass fraction was also evident in MT- and SQT-SOA. MT-SOA shows that the mass fraction is distributed between C_7-C_{10} molecules as also reported by Gkatzelis et al. (2018a). Its major contribution is attributed mainly to C_9 and C_{10} ions, reaching up to 48%, with C_7-C_9 ions accounting for about ~37%. Oxygenated molecules (O_3-O_4) comprise most of the SOA mass detected by PTRMS-CHARON. The distribution of the detected ions is more homogeneous than the distribution seen in non-IEPOX-SOA, which may be influenced by a degree of fragmentation of larger molecules. This same behavior was also identified in

the SQT-SOA where its contribution is more evenly distributed as a function of carbon number. The highest contribution is in C_{15} molecules, followed by C_7-C_9 and C_{14}. Highly oxygenated compounds were also important in the fraction of SOA. The O_3-O_4 molecules contribute ~50 % of the SOA fraction during β-caryophyllene ozonolysis.

4. Conclusions

This study presents the first systematic characterization of biogenic SOA formation using the PTRMS-CHARON inlet coupled to the new DouAir atmospheric simulation chamber. By investigating five distinct formation pathways: isoprene OH oxidation (HO_2-channel favoring and suppressing IEPOX, and the high-NO pathway), as well as monoterpene (limonene) and sesquiterpene (β-caryophyllene) ozonolysis, we established a comprehensive reference library of mass spectral fingerprints. The results reveal distinct chemical signatures for each pathway.

For isoprene, we successfully distinguished between the two low-NO regimes. The ISOP-IEPOX-SOA spectrum was characterized by well-known tracers such as $C_5H_{10}O_3$ (*m/z* 119.07) and $C_5H_{12}O_4$ (*m/z* 137.081). Furthermore, this pathway exhibited a broad and complex molecular distribution, likely driven by the decomposition and ionic fragmentation of low-volatility oligomers formed under acidic conditions. In contrast, ISOP-non-IEPOX-SOA was dominated by highly oxidized C_5 products, specifically $C_5H_{10}O_4$ and $C_5H_{10}O_6$.

A critical finding for future source apportionment is the behavior of the C_5H_6O ion (*m/z* 83.049). While traditionally used as a specific IEPOX tracer in AMS measurements, our PTRMS-CHARON data detected this ion in both low-NO isoprene pathways. This suggests that within the CHARON ionization context, C_5H_6O acts as a broader tracer for low-NO isoprene SOA rather than a unique marker for the IEPOX route. Consequently, caution is warranted when attributing this signal exclusively to IEPOX-SOA in ambient CHARON datasets.

The ozonolysis of monoterpenes and sesquiterpenes yielded spectra dominated by C_7-C_{10} and C_{11}-C_{15} oxidation products, respectively. In both cases, the presence of characteristic fragments ($[M+H-H_2O]^+$) was significant. This highlights the importance of accounting for ionic fragmentation when interpreting PTRMS-CHARON spectra, particularly for semi-volatile species that may undergo dehydration in the drift tube.

Overall, this work provides a robust experimental framework and a spectral database that enhances the capability of PTRMS-CHARON for source identification. These reference spectra will be essential for disentangling complex ambient mixtures in forested and urbanized environments, offering a higher molecular-level resolution than traditional bulk aerosol monitoring techniques.

Author contributions. CRR, OM, and JFB designed the chamber experiments. CRR, OM, HB, LF, and MJ carried out experiments and supervised the laboratory work. JFB, CP, and SS supervised the scientific work. CRR and OM analysed the data. CRR wrote the manuscript with contributions from all coauthors.

Competing interests. The contact author has declared that none of the authors has any competing interests.

Acknowledgments

Financial support. IMT Nord Europe acknowledges financial support from CPER ECRIN project funded by the Regional Council "Hauts-de-France", the European Regional Development Fund (ERDF). The French State

under the France-2030 programme and the Initiative of Excellence of the University of Lille are acknowledged for the funding and support granted to the R-CDP-24-003-AREA project. Max Planck Institute for Chemistry acknowledges financial support from the Max Planck Society and the Bundesministerium für Bildung und Forschung (BMBF contract 01LK2101B).

References

Armstrong, N. C., Chen, Y., Cui, T., Zhang, Y., Christensen, C., Zhang, Z., Turpin, B. J., Chan, M. N., Gold, A., Ault, A. P., and Surratt, J. D.: Isoprene Epoxydiol-Derived Sulfated and Nonsulfated Oligomers Suppress Particulate Mass Loss during Oxidative Aging of Secondary Organic Aerosol, Environ. Sci. Technol, 56, 16611–16620, https://doi.org/10.1021/acs.est.2c03200, 2022.

Barmet, P., Dommen, J., DeCarlo, P. F., Tritscher, T., Praplan, A. P., Platt, S. M., Prévôt, A. S. H., Donahue, N. M., and Baltensperger, U.: OH clock determination by proton transfer reaction mass spectrometry at an environmental chamber, Atmos. Meas. Tech., 5, 647–656, https://doi.org/10.5194/amt-5-647-2012, 2012.

Berndt, T., Hyttinen, N., Herrmann, H., and Hansel, A.: First oxidation products from the reaction of hydroxyl radicals with isoprene for pristine environmental conditions, Commun. Chem., 2, 21, https://doi.org/10.1038/s42004-019-0120-9, 2019.

Bernhammer, A.-K., Breitenlechner, M., Keutsch, F. N., and Hansel, A.: Technical note: Conversion of isoprene hydroxy hydroperoxides (ISOPOOHs) on metal environmental simulation chamber walls, Atmos. Chem. Phys., 17, 4053–4062, https://doi.org/10.5194/acp-17-4053-2017, 2017.

Budisulistiorini, S. H., Canagaratna, M. R., Croteau, P. L., Marth, W. J., Baumann, K., Edgerton, E. S., Shaw, S. L., Knipping, E. M., Worsnop, D. R., Jayne, J. T., Gold, A., and Surratt, J. D.: Real-Time Continuous Characterization of Secondary Organic Aerosol Derived from Isoprene Epoxydiols in Downtown Atlanta, Georgia, Using the Aerodyne Aerosol Chemical Speciation Monitor, Environ. Sci. Technol, 47, 5686–5694, https://doi.org/10.1021/es400023n, 2013.

Canagaratna, M. R., Jimenez, J. L., Kroll, J. H., Chen, Q., Kessler, S. H., Massoli, P., Hildebrandt Ruiz, L., Fortner, E., Williams, L. R., Wilson, K. R., Surratt, J. D., Donahue, N. M., Jayne, J. T., and Worsnop, D. R.: Elemental ratio measurements of organic compounds using aerosol mass spectrometry: characterization, improved calibration, and implications, Atmos. Chem. Phys., 15, 253–272, https://doi.org/10.5194/acp-15-253-2015, 2015.

Chan, A. W. H., Chan, M. N., Surratt, J. D., Chhabra, P. S., Loza, C. L., Crounse, J. D., Yee, L. D., Flagan, R. C., Wennberg, P. O., and Seinfeld, J. H.: Role of aldehyde chemistry and NO_x concentrations in secondary organic aerosol formation, Atmos. Chem. Phys., 10, 7169–7188, https://doi.org/10.5194/acp-10-7169-2010, 2010.

Chan, M. N., Surratt, J. D., Chan, A. W. H., Schilling, K., Offenberg, J. H., Lewandowski, M., Edney, E. O., Kleindienst, T. E., Jaoui, M., Edgerton, E. S., Tanner, R. L., Shaw, S. L., Zheng, M., Knipping, E. M., and

Seinfeld, J. H.: Influence of aerosol acidity on the chemical composition of secondary organic aerosol from β-caryophyllene, Atmos. Chem. Phys., 11, 1735–1751, https://doi.org/10.5194/acp-11-1735-2011, 2011.

Cubison, M. J., Ortega, A. M., Hayes, P. L., Farmer, D. K., Day, D., Lechner, M. J., Brune, W. H., Apel, E., Diskin, G. S., Fisher, J. A., Fuelberg, H. E., Hecobian, A., Knapp, D. J., Mikoviny, T., Riemer, D., Sachse, G. W., Sessions, W., Weber, R. J., Weinheimer, A. J., Wisthaler, A., and Jimenez, J. L.: Effects of aging on organic aerosol from open biomass burning smoke in aircraft and laboratory studies, Atmos. Chem. Phys., 11, 12049–12064, https://doi.org/10.5194/acp-11-12049-2011, 2011.

D'Ambro, E. L., Lee, B. H., Liu, J., Shilling, J. E., Gaston, C. J., Lopez-Hilfiker, F. D., Schobesberger, S., Zaveri, R. A., Mohr, C., Lutz, A., Zhang, Z., Gold, A., Surratt, J. D., Rivera-Rios, J. C., Keutsch, F. N., and Thornton, J. A.: Molecular composition and volatility of isoprene photochemical oxidation secondary organic aerosol under low- and high-NO_x conditions, Atmos. Chem. Phys., 17, 159–174, https://doi.org/10.5194/acp-17-159-2017, 2017.

D'Ambro, E. L., Schobesberger, S., Gaston, C. J., Lopez-Hilfiker, F. D., Lee, B. H., Liu, J., Zelenyuk, A., Bell, D., Cappa, C. D., Helgestad, T., Li, Z., Guenther, A., Wang, J., Wise, M., Caylor, R., Surratt, J. D., Riedel, T., Hyttinen, N., Salo, V.-T., Hasan, G., Kurtén, T., Shilling, J. E., and Thornton, J. A.: Chamber-based insights into the factors controlling epoxydiol (IEPOX) secondary organic aerosol (SOA) yield, composition, and volatility, Atmos. Chem. Phys., 19, 11253–11265, https://doi.org/10.5194/acp-19-11253-2019, 2019.

Dada, L., Stolzenburg, D., Simon, M., Fischer, L., Heinritzi, M., Wang, M., Xiao, M., Vogel, A. L., Ahonen, L., Amorim, A., Baalbaki, R., Baccarini, A., Baltensperger, U., Bianchi, F., Daellenbach, K. R., DeVivo, J., Dias, A., Dommen, J., Duplissy, J., Finkenzeller, H., Hansel, A., He, X.-C., Hofbauer, V., Hoyle, C. R., Kangasluoma, J., Kim, C., Kürten, A., Kvashnin, A., Mauldin, R., Makhmutov, V., Marten, R., Mentler, B., Nie, W., Petäjä, T., Quéléver, L. L. J., Saathoff, H., Tauber, C., Tome, A., Molteni, U., Volkamer, R., Wagner, R., Wagner, A. C., Wimmer, D., Winkler, P. M., Yan, C., Zha, Q., Rissanen, M., Gordon, H., Curtius, J., Worsnop, D. R., Lehtipalo, K., Donahue, N. M., Kirkby, J., Haddad, I. El, and Kulmala, M.: Role of sesquiterpenes in biogenic new particle formation, Sci. Adv., 9, eadi5297, https://doi.org/10.1126/sciadv.adi5297, 2023.

DeCarlo, P. F., Kimmel, J. R., Trimborn, A., Northway, M. J., Jayne, J. T., Aiken, A. C., Gonin, M., Fuhrer, K., Horvath, T., Docherty, K. S., Worsnop, D. R., and Jimenez, J. L.: Field-deployable, high-resolution, time-of-flight aerosol mass spectrometer., Anal. Chem., 78, 8281–8289, https://doi.org/10.1021/ac061249n, 2006.

Eichler, P., Müller, M., D'Anna, B., and Wisthaler, A.: A novel inlet system for online chemical analysis of semi-volatile submicron particulate matter, Atmos. Meas. Tech., 8, 1353–1360, https://doi.org/10.5194/amt-8-1353-2015, 2015.

Frauenheim, M., Offenberg, J., Zhang, Z., Surratt, J. D., and Gold, A.: The C_5–Alkene Triol Conundrum: Structural Characterization and Quantitation of Isoprene-Derived $C_5H_{10}O_3$ Reactive Uptake Products, Environ. Sci. Technol Lett., 9, 829–836, https://doi.org/10.1021/acs.estlett.2c00548, 2022.

Gao, L., Song, J., Mohr, C., Huang, W., Vallon, M., Jiang, F., Leisner, T., and Saathoff, H.: Kinetics, SOA yields, and chemical composition of secondary organic aerosol from β-caryophyllene ozonolysis with and without nitrogen oxides between 213 and 313 K, Atmos. Chem. Phys., 22, 6001–6020, https://doi.org/10.5194/acp-22-6001-2022, 2022.

Gkatzelis, G. I., Tillmann, R., Hohaus, T., Müller, M., Eichler, P., Xu, K.-M., Schlag, P., Schmitt, S. H., Wegener, R., Kaminski, M., Holzinger, R., Wisthaler, A., and Kiendler-Scharr, A.: Comparison of three aerosol chemical characterization techniques utilizing PTR-ToF-MS: a study on freshly formed and aged biogenic SOA, Atmos. Meas. Tech., 11, 1481–1500, https://doi.org/10.5194/amt-11-1481-2018, 2018a.

Gkatzelis, G. I., Hohaus, T., Tillmann, R., Gensch, I., Müller, M., Eichler, P., Xu, K.-M., Schlag, P., Schmitt, S. H., Yu, Z., Wegener, R., Kaminski, M., Holzinger, R., Wisthaler, A., and Kiendler-Scharr, A.: Gas-to-particle partitioning of major biogenic oxidation products: a study on freshly formed and aged biogenic SOA, Atmos. Chem. Phys., 18, 12969–12989, https://doi.org/10.5194/acp-18-12969-2018, 2018b.

de Gouw, J. and Jimenez, J. L.: Organic Aerosols in the Earth's Atmosphere, Environ. Sci. Technol, 43, 7614–7618, https://doi.org/10.1021/es9006004, 2009.

de Gouw, J. and Warneke, C.: Measurements of volatile organic compounds in the earth's atmosphere using proton-transfer-reaction mass spectrometry, Mass Spectrom. Rev., 26, 223–257, https://doi.org/https://doi.org/10.1002/mas.20119, 2007.

Hakola, H., Hellén, H., Hemmilä, M., Rinne, J., and Kulmala, M.: In situ measurements of volatile organic compounds in a boreal forest, Atmos. Chem. Phys., 12, 11665–11678, https://doi.org/10.5194/acp-12-11665-2012, 2012.

Hallquist, M., Wenger, J. C., Baltensperger, U., Rudich, Y., Simpson, D., Claeys, M., Dommen, J., Donahue, N. M., George, C., Goldstein, A. H., Hamilton, J. F., Herrmann, H., Hoffmann, T., Iinuma, Y., Jang, M., Jenkin, M. E., Jimenez, J. L., Kiendler-Scharr, A., Maenhaut, W., McFiggans, G., Mentel, T. F., Monod, A., Prévôt, A. S. H., Seinfeld, J. H., Surratt, J. D., Szmigielski, R., and Wildt, J.: The formation, properties and impact of secondary organic aerosol: current and emerging issues, Atmos. Chem. Phys., 9, 5155–5236, https://doi.org/10.5194/acp-9-5155-2009, 2009.

Hammes, J., Lutz, A., Mentel, T., Faxon, C., and Hallquist, M.: Carboxylic acids from limonene oxidation by ozone and hydroxyl radicals: insights into mechanisms derived using a FIGAERO-CIMS, Atmos. Chem. Phys., 19, 13037–13052, https://doi.org/10.5194/acp-19-13037-2019, 2019.

Hu, W. W., Campuzano-Jost, P., Palm, B. B., Day, D. A., Ortega, A. M., Hayes, P. L., Krechmer, J. E., Chen, Q., Kuwata, M., Liu, Y. J., de Sá, S. S., McKinney, K., Martin, S. T., Hu, M., Budisulistiorini, S. H., Riva, M., Surratt, J. D., St. Clair, J. M., Isaacman-Van Wertz, G., Yee, L. D., Goldstein, A. H., Carbone, S., Brito, J., Artaxo, P., de Gouw, J. A., Koss, A., Wisthaler, A., Mikoviny, T., Karl, T., Kaser, L., Jud, W., Hansel, A., Docherty, K. S., Alexander, M. L., Robinson, N. H., Coe, H., Allan, J. D., Canagaratna, M. R., Paulot, F., and Jimenez, J. L.:

Characterization of a real-time tracer for isoprene epoxydiols-derived secondary organic aerosol (IEPOX-SOA) from aerosol mass spectrometer measurements, Atmos. Chem. Phys., 15, 11807–11833, https://doi.org/10.5194/acp-15-11807-2015, 2015.

Huang, W., Li, H., Sarnela, N., Heikkinen, L., Tham, Y. J., Mikkilä, J., Thomas, S. J., Donahue, N. M., Kulmala, M., and Bianchi, F.: Measurement report: Molecular composition and volatility of gaseous organic compounds in a boreal forest - from volatile organic compounds to highly oxygenated organic molecules, Atmos. Chem. Phys., 21, 8961–8977, https://doi.org/10.5194/acp-21-8961-2021, 2021.

Jacob, F., Houzel, N., Genevray, P., Clety, C., Coeur, C., Perdrix, E., Alleman, L. Y., Anthérieu, S., Garçon, G., Dhont, G., Cuisset, A., Lo Guidice, J.-M., and Tomas, A.: New insights into the chemical composition and formation mechanisms of secondary organic aerosols produced in the ozonolysis of limonene, J. Aerosol Sci., 173, 106214, https://doi.org/https://doi.org/10.1016/j.jaerosci.2023.106214, 2023.

Jacobs, M. I., Burke, W. J., and Elrod, M. J.: Kinetics of the reactions of isoprene-derived hydroxynitrates: gas phase epoxide formation and solution phase hydrolysis, Atmos. Chem. Phys., 14, 8933–8946, https://doi.org/10.5194/acp-14-8933-2014, 2014.

Jaoui, M., Kleindienst, T. E., Docherty, K. S., Lewandowski, M., and Offenberg, J. H.: Secondary organic aerosol formation from the oxidation of a series of sesquiterpenes: α-cedrene, β-caryophyllene, α-humulene and α-farnesene with O_3, OH and NO_3 radicals, Environ. Chem., 10, 178–193, 2013.

Jia, L. and Xu, Y.: Different roles of water in secondary organic aerosol formation from toluene and isoprene, Atmos. Chem. Phys., 18, 8137–8154, https://doi.org/10.5194/acp-18-8137-2018, 2018.

Kim, S., Karl, T., Helmig, D., Daly, R., Rasmussen, R., and Guenther, A.: Measurement of atmospheric sesquiterpenes by proton transfer reaction-mass spectrometry (PTR-MS), Atmos. Meas. Tech., 2, 99–112, https://doi.org/10.5194/amt-2-99-2009, 2009.

Kleindienst, T. E., Jaoui, M., Lewandowski, M., Offenberg, J. H., Lewis, C. W., Bhave, P. V, and Edney, E. O.: Estimates of the contributions of biogenic and anthropogenic hydrocarbons to secondary organic aerosol at a southeastern US location, Atmos. Environ., 41, 8288–8300, https://doi.org/https://doi.org/10.1016/j.atmosenv.2007.06.045, 2007.

Kostenidou, E., Marques, B., Temime-Roussel, B., Liu, Y., Vansevenant, B., Sartelet, K., and D'Anna, B.: Secondary organic aerosol formed by Euro 5 gasoline vehicle emissions: chemical composition and gas-to-particle phase partitioning, Atmos. Chem. Phys., 24, 2705–2729, https://doi.org/10.5194/acp-24-2705-2024, 2024.

Krechmer, J. E., Coggon, M. M., Massoli, P., Nguyen, T. B., Crounse, J. D., Hu, W., Day, D. A., Tyndall, G. S., Henze, D. K., Rivera-Rios, J. C., Nowak, J. B., Kimmel, J. R., Mauldin, R. L. I. I. I., Stark, H., Jayne, J. T., Sipilä, M., Junninen, H., St. Clair, J. M., Zhang, X., Feiner, P. A., Zhang, L., Miller, D. O., Brune, W. H., Keutsch, F. N., Wennberg, P. O., Seinfeld, J. H., Worsnop, D. R., Jimenez, J. L., and Canagaratna, M. R.: Formation of

Low Volatility Organic Compounds and Secondary Organic Aerosol from Isoprene Hydroxyhydroperoxide Low-NO Oxidation, Environ. Sci. Technol, 49, 10330–10339, https://doi.org/10.1021/acs.est.5b02031, 2015.

Kristensen, K., Jensen, L. N., Glasius, M., and Bilde, M.: The effect of sub-zero temperature on the formation and composition of secondary organic aerosol from ozonolysis of alpha-pinene, Environ. Sci. Process. Impacts, 19, 1220–1234, https://doi.org/10.1039/C7EM00231A, 2017.

Kundu, S., Fisseha, R., Putman, A. L., Rahn, T. A., and Mazzoleni, L. R.: High molecular weight SOA formation during limonene ozonolysis: insights from ultrahigh-resolution FT-ICR mass spectrometry characterization, Atmos. Chem. Phys., 12, 5523–5536, https://doi.org/10.5194/acp-12-5523-2012, 2012.

Kuwata, M., Liu, Y., McKinney, K., and Martin, S. T.: Physical state and acidity of inorganic sulfate can regulate the production of secondary organic material from isoprene photooxidation products, Phys. Chem. Chem. Phys., 17, 5670–5678, https://doi.org/10.1039/C4CP04942J, 2015.

Lannuque, V., D'Anna, B., Kostenidou, E., Couvidat, F., Martinez-Valiente, A., Eichler, P., Wisthaler, A., Müller, M., Temime-Roussel, B., Valorso, R., and Sartelet, K.: Gas-particle partitioning of toluene oxidation products: an experimental and modeling study, EGUsphere, 2023, 1–36, https://doi.org/10.5194/egusphere-2023-1290, 2023.

Leppla, D., Hildmann, S., Zannoni, N., Kremper, L., Hollanda, B., Williams, J., Pöhlker, C., Wolff, S., Sà, M., Solci, M. C., Pöschl, U., and Hoffmann, T.: Comprehensive Non-targeted Molecular Characterization of Organic Aerosols in the Amazon Rainforest, EGUsphere, 2025, 1–32, https://doi.org/10.5194/egusphere-2025-141, 2025.

Li, Y. J., Chen, Q., Guzman, M. I., Chan, C. K., and Martin, S. T.: Second-generation products contribute substantially to the particle-phase organic material produced by β-caryophyllene ozonolysis, Atmos. Chem. Phys., 11, 121–132, https://doi.org/10.5194/acp-11-121-2011, 2011.

Lin, Y.-H., Zhang, Z., Docherty, K. S., Zhang, H., Budisulistiorini, S. H., Rubitschun, C. L., Shaw, S. L., Knipping, E. M., Edgerton, E. S., Kleindienst, T. E., Gold, A., and Surratt, J. D.: Isoprene Epoxydiols as Precursors to Secondary Organic Aerosol Formation: Acid-Catalyzed Reactive Uptake Studies with Authentic Compounds, Environ. Sci. Technol, 46, 250–258, https://doi.org/10.1021/es202554c, 2012.

Lin, Y.-H., Zhang, H., Pye, H. O. T., Zhang, Z., Marth, W. J., Park, S., Arashiro, M., Cui, T., Budisulistiorini, S. H., Sexton, K. G., Vizuete, W., Xie, Y., Luecken, D. J., Piletic, I. R., Edney, E. O., Bartolotti, L. J., Gold, A., and Surratt, J. D.: Epoxide as a precursor to secondary organic aerosol formation from isoprene photooxidation in the presence of nitrogen oxides, Proc. Natl. Acad. Sci., 110, 6718–6723, https://doi.org/10.1073/pnas.1221150110, 2013.

Lin, Y.-H., Budisulistiorini, S. H., Chu, K., Siejack, R. A., Zhang, H., Riva, M., Zhang, Z., Gold, A., Kautzman, K. E., and Surratt, J. D.: Light-Absorbing Oligomer Formation in Secondary Organic Aerosol from

Reactive Uptake of Isoprene Epoxydiols, Environ. Sci. Technol, 48, 12012–12021, https://doi.org/10.1021/es503142b, 2014.

Liu, J., D'Ambro, E. L., Lee, B. H., Lopez-Hilfiker, F. D., Zaveri, R. A., Rivera-Rios, J. C., Keutsch, F. N., Iyer, S., Kurten, T., Zhang, Z., Gold, A., Surratt, J. D., Shilling, J. E., and Thornton, J. A.: Efficient Isoprene Secondary Organic Aerosol Formation from a Non-IEPOX Pathway, Environ. Sci. Technol, 50, 9872–9880, https://doi.org/10.1021/acs.est.6b01872, 2016.

Liu, Y., Kuwata, M., Strick, B. F., Geiger, F. M., Thomson, R. J., McKinney, K. A., and Martin, S. T.: Uptake of Epoxydiol Isomers Accounts for Half of the Particle-Phase Material Produced from Isoprene Photooxidation via the HO_2 Pathway, Environ. Sci. Technol, 49, 250–258, https://doi.org/10.1021/es5034298, 2015.

Liu, Y. J., Herdlinger-Blatt, I., McKinney, K. A., and Martin, S. T.: Production of methyl vinyl ketone and methacrolein via the hydroperoxyl pathway of isoprene oxidation, Atmos. Chem. Phys., 13, 5715–5730, https://doi.org/10.5194/acp-13-5715-2013, 2013.

Lopez-Hilfiker, F. D., Mohr, C., Ehn, M., Rubach, F., Kleist, E., Wildt, J., Mentel, T. F., Lutz, A., Hallquist, M., Worsnop, D., and Thornton, J. A.: A novel method for online analysis of gas and particle composition: description and evaluation of a Filter Inlet for Gases and AEROsols (FIGAERO), Atmos. Meas. Tech., 7, 983–1001, https://doi.org/10.5194/amt-7-983-2014, 2014.

Lopez-Hilfiker, F. D., Mohr, C., D'Ambro, E. L., Lutz, A., Riedel, T. P., Gaston, C. J., Iyer, S., Zhang, Z., Gold, A., Surratt, J. D., Lee, B. H., Kurten, T., Hu, W. W. W., Jimenez, J., Hallquist, M., Thornton, J. A., D'Ambro, E. L., Lutz, A., Riedel, T. P., Gaston, C. J., Iyer, S., Zhang, Z., Gold, A., Surratt, J. D., Lee, B. H., Kurten, T., Hu, W. W. W., Jimenez, J., Hallquist, M., and Thornton, J. A.: Molecular Composition and Volatility of Organic Aerosol in the Southeastern U.S.: Implications for IEPOX Derived SOA, Environ. Sci. Technol., 50, 2200–2209, https://doi.org/10.1021/acs.est.5b04769, 2016.

Martin, S. T., Andreae, M. O., Althausen, D., Artaxo, P., Baars, H., Borrmann, S., Chen, Q., Farmer, D. K., Guenther, A., Gunthe, S. S., Jimenez, J. L., Karl, T., Longo, K., Manzi, A., Müller, T., Pauliquevis, T., Petters, M. D., Prenni, A. J., Pöschl, U., Rizzo, L. V, Schneider, J., Smith, J. N., Swietlicki, E., Tota, J., Wang, J., Wiedensohler, A., and Zorn, S. R.: An overview of the Amazonian Aerosol Characterization Experiment 2008 (AMAZE-08), Atmos. Chem. Phys., 10, 11415–11438, https://doi.org/10.5194/acp-10-11415-2010, 2010.

Mettke, P., Brüggemann, M., Mutzel, A., Gräfe, R., and Herrmann, H.: Secondary Organic Aerosol (SOA) through Uptake of Isoprene Hydroxy Hydroperoxides (ISOPOOH) and its Oxidation Products, ACS Earth Sp. Chem., 7, 1025–1037, https://doi.org/10.1021/acsearthspacechem.2c00385, 2023.

Michoud, V., Sciare, J., Sauvage, S., Dusanter, S., Léonardis, T., Gros, V., Kalogridis, C., Zannoni, N., Féron, A., Petit, J.-E., Crenn, V., Baisnée, D., Sarda-Estève, R., Bonnaire, N., Marchand, N., DeWitt, H. L., Pey, J., Colomb, A., Gheusi, F., Szidat, S., Stavroulas, I., Borbon, A., and Locoge, N.: Organic carbon at a remote site of the western Mediterranean Basin: sources and chemistry during the ChArMEx SOP2 field experiment, Atmos.

Chem. Phys., 17, 8837–8865, https://doi.org/10.5194/acp-17-8837-2017, 2017.

Middlebrook, A. M., Bahreini, R., Jimenez, J. L., and Canagaratna, M. R.: Evaluation of Composition-Dependent Collection Efficiencies for the Aerodyne Aerosol Mass Spectrometer using Field Data, Aerosol Sci. Technol., 46, 258–271, https://doi.org/10.1080/02786826.2011.620041, 2012.

Milic, A., Mallet, M. D., Cravigan, L. T., Alroe, J., Ristovski, Z. D., Selleck, P., Lawson, S. J., Ward, J., Desservettaz, M. J., Paton-Walsh, C., Williams, L. R., Keywood, M. D., and Miljevic, B.: Biomass burning and biogenic aerosols in northern Australia during the SAFIRED campaign, Atmos. Chem. Phys., 17, 3945–3961, https://doi.org/10.5194/acp-17-3945-2017, 2017.

Morgan, W. T., Allan, J. D., Bauguitte, S., Darbyshire, E., Flynn, M. J., Lee, J., Liu, D., Johnson, B., Haywood, J., Longo, K. M., Artaxo, P. E., and Coe, H.: Transformation and ageing of biomass burning carbonaceous aerosol over tropical South America from aircraft in situ measurements during SAMBBA, Atmos. Chem. Phys., 20, 5309–5326, https://doi.org/10.5194/acp-20-5309-2020, 2020.

Müller, M., Mikoviny, T., Feil, S., Haidacher, S., Hanel, G., Hartungen, E., Jordan, A., Märk, L., Mutschlechner, P., Schottkowsky, R., Sulzer, P., Crawford, J. H., and Wisthaler, A.: A compact PTR-ToF-MS instrument for airborne measurements of volatile organic compounds at high spatiotemporal resolution, Atmos. Meas. Tech., 7, 3763–3772, https://doi.org/10.5194/amt-7-3763-2014, 2014.

Müller, M., Eichler, P., D'Anna, B., Tan, W., and Wisthaler, A.: Direct Sampling and Analysis of Atmospheric Particulate Organic Matter by Proton-Transfer-Reaction Mass Spectrometry, Anal. Chem., 89, 10889–10897, https://doi.org/10.1021/acs.analchem.7b02582, 2017.

Nault, B. A., Jo, D. S., McDonald, B. C., Campuzano-Jost, P., Day, D. A., Hu, W., Schroder, J. C., Allan, J., Blake, D. R., Canagaratna, M. R., Coe, H., Coggon, M. M., DeCarlo, P. F., Diskin, G. S., Dunmore, R., Flocke, F., Fried, A., Gilman, J. B., Gkatzelis, G., Hamilton, J. F., Hanisco, T. F., Hayes, P. L., Henze, D. K., Hodzic, A., Hopkins, J., Hu, M., Huey, L. G., Jobson, B. T., Kuster, W. C., Lewis, A., Li, M., Liao, J., Nawaz, M. O., Pollack, I. B., Peischl, J., Rappenglück, B., Reeves, C. E., Richter, D., Roberts, J. M., Ryerson, T. B., Shao, M., Sommers, J. M., Walega, J., Warneke, C., Weibring, P., Wolfe, G. M., Young, D. E., Yuan, B., Zhang, Q., de Gouw, J. A., and Jimenez, J. L.: Secondary organic aerosols from anthropogenic volatile organic compounds contribute substantially to air pollution mortality, Atmos. Chem. Phys., 21, 11201–11224, https://doi.org/10.5194/acp-21-11201-2021, 2021.

Nguyen, T. B., Roach, P. J., Laskin, J., Laskin, A., and Nizkorodov, S. A.: Effect of humidity on the composition of isoprene photooxidation secondary organic aerosol, Atmos. Chem. Phys., 11, 6931–6944, https://doi.org/10.5194/acp-11-6931-2011, 2011.

Peng, Y., Wang, H., Gao, Y., Jing, S., Zhu, S., Huang, D., Hao, P., Lou, S., Cheng, T., Huang, C., and Zhang, X.: Real-time measurement of phase partitioning of organic compounds using a proton-transfer-reaction time-of-flight mass spectrometer coupled to a CHARON inlet, Atmos. Meas. Tech., 16, 15–28,

https://doi.org/10.5194/amt-16-15-2023, 2023.

Piel, F., Müller, M., Mikoviny, T., Pusede, S. E., and Wisthaler, A.: Airborne measurements of particulate organic matter by proton-transfer-reaction mass spectrometry (PTR-MS): a pilot study, Atmos. Meas. Tech., 12, 5947–5958, https://doi.org/10.5194/amt-12-5947-2019, 2019.

Pye, H., Ward-Caviness, C., Murphy, B., Appel, W., and Seltzer, K.: Secondary organic aerosol association with cardiorespiratory disease mortality in the United States, Nat. Commun., 12, https://doi.org/10.1038/s41467-021-27484-1, 2021.

Robinson, N. H., Hamilton, J. F., Allan, J. D., Langford, B., Oram, D. E., Chen, Q., Docherty, K., Farmer, D. K., Jimenez, J. L., Ward, M. W., Hewitt, C. N., Barley, M. H., Jenkin, M. E., Rickard, A. R., Martin, S. T., McFiggans, G., and Coe, H.: Evidence for a significant proportion of Secondary Organic Aerosol from isoprene above a maritime tropical forest, Atmos. Chem. Phys., 11, 1039–1050, https://doi.org/10.5194/acp-11-1039-2011, 2011.

Roldin, P., Ehn, M., Kurtén, T., Olenius, T., Rissanen, M. P., Sarnela, N., Elm, J., Rantala, P., Hao, L., Hyttinen, N., Heikkinen, L., Worsnop, D. R., Pichelstorfer, L., Xavier, C., Clusius, P., Öström, E., Petäjä, T., Kulmala, M., Vehkamäki, H., Virtanen, A., Riipinen, I., and Boy, M.: The role of highly oxygenated organic molecules in the Boreal aerosol-cloud-climate system, Nat. Commun., 10, 4370, https://doi.org/10.1038/s41467-019-12338-8, 2019.

Schwantes, R. H., Charan, S. M., Bates, K. H., Huang, Y., Nguyen, T. B., Mai, H., Kong, W., Flagan, R. C., and Seinfeld, J. H.: Low-volatility compounds contribute significantly to isoprene secondary organic aerosol (SOA) under high-NO_x conditions, Atmos. Chem. Phys., 19, 7255–7278, https://doi.org/10.5194/acp-19-7255-2019, 2019.

Shrivastava, M., Cappa, C. D., Fan, J., Goldstein, A. H., Guenther, A. B., Jimenez, J. L., Kuang, C., Laskin, A., Martin, S. T., Ng, N. L., Petaja, T., Pierce, J. R., Rasch, P. J., Roldin, P., Seinfeld, J. H., Shilling, J., Smith, J. N., Thornton, J. A., Volkamer, R., Wang, J., Worsnop, D. R., Zaveri, R. A., Zelenyuk, A., and Zhang, Q.: Recent advances in understanding secondary organic aerosol: Implications for global climate forcing, Rev. Geophys., 55, 509–559, https://doi.org/https://doi.org/10.1002/2016RG000540, 2017.

Song, J., Saathoff, H., Jiang, F., Gao, L., Zhang, H., and Leisner, T.: Sources of organic gases and aerosol particles and their roles in nighttime particle growth at a rural forested site in southwest Germany, Atmos. Chem. Phys., 24, 6699–6717, https://doi.org/10.5194/acp-24-6699-2024, 2024.

Surratt, J. D., Murphy, S. M., Kroll, J. H., Ng, N. L., Hildebrandt, L., Sorooshian, A., Szmigielski, R., Vermeylen, R., Maenhaut, W., Claeys, M., Flagan, R. C., and Seinfeld, J. H.: Chemical Composition of Secondary Organic Aerosol Formed from the Photooxidation of Isoprene, J. Phys. Chem. A, 110, 9665–9690, https://doi.org/10.1021/jp061734m, 2006.

Tsimpidi, A. P., Scholz, S. M. C., Milousis, A., Mihalopoulos, N., and Karydis, V. A.: Aerosol composition trends during 2000-2020: in-depth insights from model predictions and multiple worldwide near-surface observation datasets, Atmos. Chem. Phys., 25, 10183–10213, https://doi.org/10.5194/acp-25-10183-2025, 2025.

Wong, C., Vite, D., and Nizkorodov, S. A.: Stability of α-Pinene and d-Limonene Ozonolysis Secondary Organic Aerosol Compounds Toward Hydrolysis and Hydration, ACS Earth Sp. Chem., 5, 2555–2564, https://doi.org/10.1021/acsearthspacechem.1c00171, 2021.

Wong, J. P. S., Lee, A. K. Y., and Abbatt, J. P. D.: Impacts of Sulfate Seed Acidity and Water Content on Isoprene Secondary Organic Aerosol Formation, Environ. Sci. Technol, 49, 13215–13221, https://doi.org/10.1021/acs.est.5b02686, 2015.

Worton, D. R., Moreno, S., O'Daly, K., and Holzinger, R.: Development of an International System of Units (SI)-traceable transmission curve reference material to improve the quantitation and comparability of proton-transfer-reaction mass-spectrometry measurements, Atmos. Meas. Tech., 16, 1061–1072, https://doi.org/10.5194/amt-16-1061-2023, 2023.

Yáñez-Serrano, A. M., Bourtsoukidis, E., Alves, E. G., Bauwens, M., Stavrakou, T., Llusià, J., Filella, I., Guenther, A., Williams, J., Artaxo, P., Sindelarova, K., Doubalova, J., Kesselmeier, J., and Peñuelas, J.: Amazonian biogenic volatile organic compounds under global change, Glob. Chang. Biol., 26, 4722–4751, https://doi.org/https://doi.org/10.1111/gcb.15185, 2020.

Zhang, H., Surratt, J. D., Lin, Y. H., Bapat, J., and Kamens, R. M.: Effect of relative humidity on SOA formation from isoprene/NO photooxidation: enhancement of 2-methylglyceric acid and its corresponding oligoesters under dry conditions, Atmos. Chem. Phys., 11, 6411–6424, https://doi.org/10.5194/acp-11-6411-2011, 2011.

Zhou, P., Ganzeveld, L., Taipale, D., Rannik, Ü., Rantala, P., Rissanen, M. P., Chen, D., and Boy, M.: Boreal forest BVOC exchange: emissions versus in-canopy sinks, Atmos. Chem. Phys., 17, 14309–14332, https://doi.org/10.5194/acp-17-14309-2017, 2017.